Waveguide Photonic Crystal Reflectors on InP-Membranes-on-Silicon

Student paper

Sander Reniers [1], Jorn van Engelen [1], Kevin Williams [1], Jos van der Tol [1], Yuqing Jiao [1]
[1] *Photonic Integration Group, Institute for Photonic Integration, Eindhoven University of Technology, PO Box 513, 5600 MB Eindhoven, The Netherlands*

e-mail: s.f.g.reniers@tue.nl

ABSTRACT

We present waveguide photonic crystal reflectors on an InP-membrane-on-silicon (IMOS). Photonic crystal holes are patterned on a waveguide using electron-beam lithography to create a broadband distributed Bragg reflector. We show simulations of these reflectors and experimental results of fabricated devices, both showing a high, free to choose reflectivity, and high quality factor Fabry-Pérot cavities. We experimentally show reflectivities >90% for the reflectors and a quality factor as high as 11,430±1,446 for a Fabry-Pérot cavity, using reflectors with a length of only 4 microns.

Keywords: photonic integrated circuits, photonic membrane, photonic crystal, waveguide reflector.

1 INTRODUCTION

The InP-membrane-on-silicon (IMOS) platform [1] consists of a 300 nm thick membrane of InP, which corresponds to the core thickness in the nanophotonic waveguides, bonded by benzocyclobutene (BCB) to a silicon carrier wafer. The thin membrane and high index contrast enable tight light confinement and small footprint devices and waveguides, the latter being 400 nm wide for the passive waveguides. Distributed Bragg reflectors (DBR) are of key importance in any (nano) photonic platform. Controllable and high reflectivity are required for creating high quality factor Fabry-Pérot cavities, e.g. for lasers. The concept of using these reflectors to create laser cavities has been previously investigated [2], with a reported simulated quality factor for the cavities of around 1,200. We experimentally demonstrate cavities with almost an order of magnitude higher quality factor. Simulation results are shown, as well as experimental results using two different measurement techniques.

2 DESIGN AND FABRICATION

The photonic crystal reflector is implemented with elliptical holes to periodically change the refractive index [3]. A taper is required for the transition between the regular waveguide (400 nm wide) to a wider waveguide section (700 nm), in which the holes are patterned. The smaller holes are included to smoothen the transition to the high index-contrast section of the reflector.

After bonding of the wafers, the substrate of the InP wafer is removed with wet etching, leaving only the 300 nm thick membrane. Typically, the core is etched to a target depth of 20 nm from the lower membrane surface. This ensures strong waveguiding while protecting the structures during subsequent processing. An image of the waveguide is shown in Fig. 1. Patterned holes in the silicon nitride mask at an intermediate step are shown in Fig. 2 for clarity. The pattern is then transferred to the semiconductor, etching the waveguide core and holes in the same etch step. In a second lithographic step, the surface grating couplers used for fiber-to-chip coupling are created. For a detailed process description, see [1].

3 SIMULATION

The photonic crystal reflectors are simulated with finite-difference time-domain software. The adiabatic taper for the transition between the normal waveguide (400 nm wide) and the reflector (700 nm wide) is not included

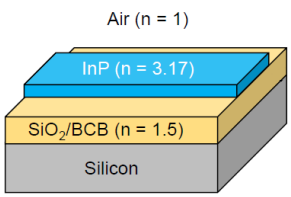

Figure 1. Example a typical IMOS waveguide.

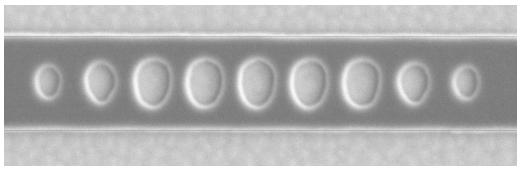

Figure 2. Scanning electron microscope (SEM) image of the photonic crystal hole reflector.

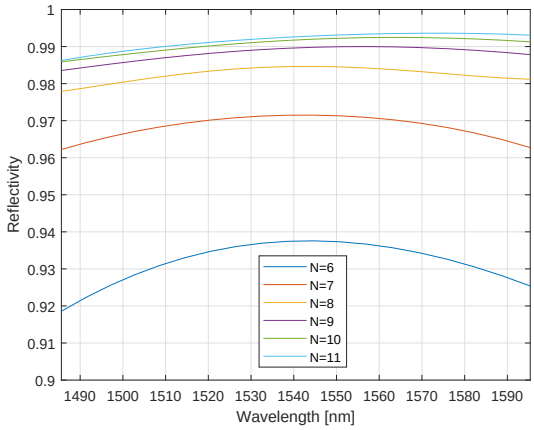

Figure 3. Simulated power reflection from a lossless photonic crystal reflector. N is the number of holes.

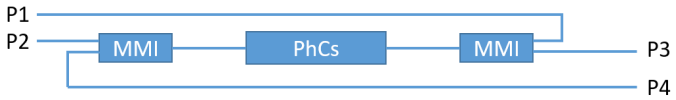

Figure 4. Schematic layout of the 4-port structure used for photonic crystal hole reflector characterization.

in the simulation model. The number of holes, which among others defines the reflectivity of the reflector, is varied for the simulation. The simulated reflection coefficients are shown in Fig. 3. From this figure, we observe that already for a low number of holes reflectivities above 90% can be expected, and even higher than 99% with an increased number of holes.

4 MEASUREMENT RESULTS AND ANALYSIS

Measurement structures for two methods of characterization are realized. The first method [4] is used to directly measure the reflectivity of a single photonic crystal reflector using a four-port measurement. For the second method, a Fabry-Pérot cavity [5] is created using two photonic crystal reflectors.

The structure that is used for the four-port measurements is schematically shown in Fig. 4. Both the power reflected by the photonic crystals holes and transmitted through the reflector can be measured in two separate measurements each. We can write the powers P_{ij} measured when the fibers are placed between port i and j as

$$P_{13} = \alpha_1\alpha_3\alpha_{\text{MMI}}^2 R P_{\text{in}}, \quad (1) \qquad P_{14} = \alpha_1\alpha_4\alpha_{\text{MMI}}^2 T P_{\text{in}}, \quad (3)$$

$$P_{23} = \alpha_2\alpha_3\alpha_{\text{MMI}}^2 T P_{\text{in}}, \quad (2) \qquad P_{24} = \alpha_2\alpha_4\alpha_{\text{MMI}}^2 R P_{\text{in}}, \quad (4)$$

where α_i is the transmission through arm i, α_{MMI} is the power transmission through the MMI ($\sim$0.5), P_{in} is the power coupled from the input fiber, R is the reflection coefficient of the reflector, and T is the transmission through the reflector. In our analysis we have assumed the reflector itself has negligible loss ($T + R = 1$), and hence we can write

$$B = \frac{P_{23}P_{14}}{P_{13}P_{24}} = \frac{(1-R)^2}{R^2}, \quad (5)$$

which gives one physical solution for the reflectivity:

$$R = \frac{1}{1+\sqrt{B}}. \quad (6)$$

In this way the measured R becomes independent of coupling and waveguide losses. By applying (5) and (6) on the measured powers P_{ij}, as given in (1)-(4), the reflection coefficient can be found for photonic crystal reflectors with various N, which is shown in Fig. 5. The shown reflection coefficients are for a lower wavelength than the targeted wavelength, which is 1550 nm. This may be understood through the wavelength-shifted transfer function for the surface grating couplers. The fringes appearing on the measurements are believed to be caused by parasitic reflections from the MMI couplers and the surface grating couplers. We observe that the reflection coefficient for a six hole reflector, over the 1490 nm to 1540 nm wavelength range, varies from 0.72 to 0.91, for an eight hole reflector it varies from 0.89 to 0.96 and for an eleven hole reflector it is above 0.96.

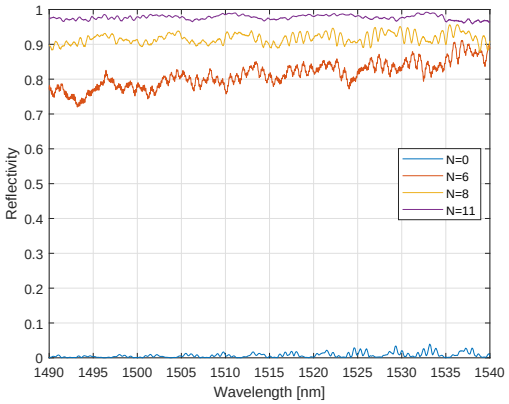

Figure 5. Reflection coefficients for photonic crystal hole reflectors with $N = 0, 6, 8, 11$, measured with the structure of Fig. 4.

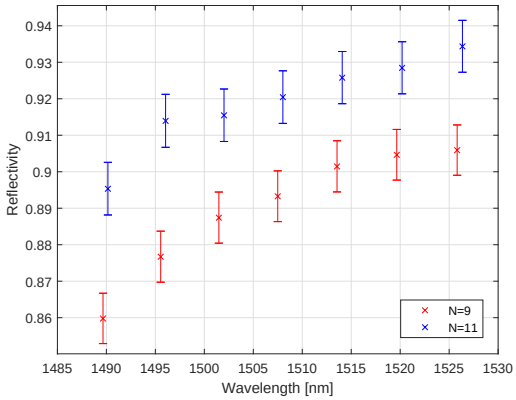

Figure 6. Reflection coefficients calculated from the Fabry-Pérot cavity measurements.

Figure 7. Schematic layout of the cavity created with two photonic crystal hole reflectors.

A Fabry-Pérot cavity is also used to measure the reflection coefficient of the photonic crystal holes, as well as the quality factor of the cavity. A schematic layout of the structure is shown in Fig. 7. The transmission spectrum for this structure is measured, and from the resonances the quality factor can be extracted by using $Q = \frac{\lambda}{\text{FWHM}}$. Furthermore, the finesse F is given by $F = \frac{\text{FSR}}{\text{FWHM}}$, and the reflection coefficient R is given by $R = \sqrt{\text{e}^{-\frac{2\pi}{F}}}$. The calculated reflection coefficients are shown in Fig. 6. The error bars on the reflectivity are due to the accuracy limits of the measurement equipment and the fringes on the measurements due to suspected parasitic reflections of the MMI couplers and the surface grating couplers. The structures with $N > 11$ could not be measured, since the transmission through the cavity was too low, probably due to the high reflectivity. The measured reflectivity is high, but somewhat lower than the values obtained from simulation, which is believed to be caused by stringent fabrication tolerances for these first prototypes.

The difference in measured reflection coefficients can be explained by the neglected losses for both measurement methods. In the four-port characterization method, the internal reflector loss is neglected, which results in a higher reflectivity. In the cavity structures, the reflector loss and the waveguide loss of the waveguide section between the two reflectors is neglected, which results in a lower derived reflectivity. The actual reflection coefficient is therefore expected to lie between these two values. An analysis on the impact of losses on the reflectivity will be presented at the conference.

5 CONCLUSION

Photonic crystal reflectors as short as 4 microns are simulated and demonstrated experimentally. Characterization of the reflectors is done using two characterization methods, both showing $> 90\%$ reflection. Therefore, the presented reflector is shown to be an important building block for our nanophotonic platform. As a result, a Fabry-Pérot cavity with a quality factor of 11,430$\pm$1,446 is experimentally demonstrated, which is very promissing for use of these cavities in lasers on IMOS.

REFERENCES

[1] J.J.G.M. van der Tol, et. al., “Indium Phosphide Integrated Photonics in Membranes,” IEEE Journal of Selected Topics in Quantum Electronics, vol. 24(1), 2018.

[2] A. Higuera Rodríguez, ”Technology Development of Nano-Scale Photonic Integrated Circuits on III-V Membranes,” PhD thesis, Eindhoven University of Technology, 2017.

[3] S.O. Kasap, ”Optoelectronics & Photonics: Principles & Practices,” Pearson, 2013.

[4] J. Pello, ”Building up a membrane photonics platform in indium phosphide,” PhD thesis, Eindhoven University of Technology, 2014.

[5] G. Hernandez, ”Fabry-Pérot Interferometers,” Cambridge University Press, 1986.